Lack of adipocyte purinergic P2Y$_6$ receptor greatly improves whole body glucose homeostasis

Shanu Jain[a], Sai P. Pydi[b], Kiran S. Toti[a], Bernard Robaye[c], Marco Idzko[d,e], Oksana Gavrilova[f], Jürgen Wess[b], and Kenneth A. Jacobson[a,1]

[a]Molecular Recognition Section, Laboratory of Bioorganic Chemistry, National Institute of Diabetes and Digestive and Kidney Diseases, Bethesda, MD 20892; [b]Molecular Signaling Section, Laboratory of Bioorganic Chemistry, National Institute of Diabetes and Digestive and Kidney Diseases, Bethesda, MD 20892; [c]Institute of Interdisciplinary Research (IRIBHM), Université Libre de Bruxelles, 6041 Gosselies, Belgium; [d]Universitätsklinik für Innere Medizin II, Klinische Abteilung für Pulmologie, Medizinische Universität, 1090 Vienna, Austria; [e]Department of Pneumology, University Hospital Freiburg, 79106 Freiburg, Germany; and [f]Mouse Metabolism Core, National Institute of Diabetes and Digestive and Kidney Diseases, Bethesda, MD 20892

Uridine diphosphate (UDP)-activated purinergic receptor P2Y$_6$ (P2Y$_6$R) plays a crucial role in controlling energy balance through central mechanisms. However, P2Y$_6$R's roles in peripheral tissues regulating energy and glucose homeostasis remain unexplored. Here, we report the surprising finding that adipocyte-specific deletion of P2Y$_6$R protects mice from diet-induced obesity, improving glucose tolerance and insulin sensitivity with reduced systemic inflammation. These changes were associated with reduced JNK signaling and enhanced expression and activity of PPARα affecting downstream PGC1α levels leading to beiging of white fat. In contrast, P2Y$_6$R deletion in skeletal muscle reduced glucose uptake, resulting in impaired glucose homeostasis. Interestingly, whole body P2Y$_6$R knockout mice showed metabolic improvements similar to those observed with mice lacking P2Y$_6$R only in adipocytes. Our findings provide compelling evidence that P2Y$_6$R antagonists may prove useful for the treatment of obesity and type 2 diabetes.

metabolism | GPCR | nucleotides | adipocyte | obesity

The increasing prevalence of obesity and type 2 diabetes (T2D) worldwide has led to added complications of cardiovascular disease, hypertension, fatty liver disease, and cancer (1, 2). Disequilibrium between caloric intake and expenditure results in excess fat storage and hence the development of obesity (3). White adipose tissue (WAT) serves as the main site for the storage of excess calories as well as an active endocrine organ that regulates glucose and energy homeostasis in an organism (4). Conversely, brown adipose tissue (BAT) is a critical adipose depot responsible for nonshivering thermogenesis and energy expenditure (4). Adipose tissue undergoes extensive morphological and functional remodeling during obesity, resulting in the development of insulin resistance, changing the repertoire of cytokines produced by the adipose tissues, and consequently increasing local and systemic inflammation (5, 6). Obesity-induced insulin resistance in other peripheral tissues such as skeletal muscle impairs glucose uptake causing hyperglycemia, thereby contributing to the core defect in T2D (7). Thus, there is an urgent need to define factors that affect the pathophysiology of adipose tissue and skeletal muscle controlling whole body (WB) energy balance and glycemic homeostasis. Identification of such factors may help to identify novel targets for the treatment of obesity and T2D.

Circulating nucleotides function as primary messengers in intercellular communication in an autocrine/paracrine manner (8). Nucleotides are released into the extracellular space in response to different pathophysiological conditions involving inflammation, cell lysis, hypoxia, trauma, and infection (9, 10). These agents play key roles in maintaining many important metabolic functions. High plasma levels of adenine and uracil nucleoside/nucleotides have been reported under conditions of obesity, acting on G protein-coupled adenosine and P2Y receptors (P2YRs) of the purinergic receptor family (11, 12). P2Y receptors such as P2Y$_1$R and P2Y$_{14}$R have been shown to play a significant role in the regulation of leptin secretion and insulin sensitivity (13, 14). G$_q$-coupled P2Y$_6$R

activation by uridine diphosphate (UDP) increases glucose uptake in adipocyte 3T3-L1 and skeletal muscle C2C12 cell lines (15). P2Y$_6$R also plays a pivotal role in inflammatory responses by stimulating immune cell migration and inducing the secretion of inflammatory cytokines such as MCP1 and IL6 (16, 17). Stresses such as environmental inflammation, chronic heart failure, and dystrophic cardiomyopathy increase P2Y$_6$R expression (18, 19). P2Y$_6$R expression has also been reported in orexigenic agouti-related peptide (AgRP)-expressing neurons in the hypothalamic arcuate nucleus (11). P2Y$_6$R-dependent activation of AgRP neurons promotes feeding in lean as well as obese mice (11). Blockade of P2Y$_6$R reduced food intake and improved insulin sensitivity in obese mice (20).

In this study, we demonstrate that P2Y$_6$R is expressed in adipose tissue and skeletal muscle and that its expression is regulated by obesity. We generated three different mouse models lacking P2Y$_6$R throughout the body or selectively in mature adipocytes or skeletal muscle cells to decipher the receptor's role in maintaining glucose and energy balance. Lack of P2Y$_6$R specifically in adipocytes led to marked improvements in glucose and insulin tolerance in mice consuming an obesogenic diet. This improvement was notably due to impaired c-Jun N-terminal kinase (JNK) activation, resulting in decreased systemic inflammation and increased browning in inguinal WAT (iWAT) lacking P2Y$_6$R.

Surprisingly, P2Y$_6$R deletion specifically in skeletal muscle impaired glucose tolerance and insulin sensitivity. This impairment was due to decreased glucose uptake in skeletal muscle lacking P2Y$_6$R. Lastly, global deletion of P2Y$_6$R improved glucose metabolism and insulin tolerance along with reducing

---

Significance

The prevalence of obesity and type 2 diabetes (T2D) has increased worldwide. Obesity is correlated with unfavorable adipose tissue modifications that lead to metabolic dysregulation. Here, we show that P2Y$_6$R deficiency in adipocytes protects from diet-induced obesity due to enhanced energy expenditure, reduced inflammation, and white adipose tissue browning. Further, adipocytes lacking P2Y$_6$R show reduced JNK expression and activity, contributing to the improved phenotype. This proof-of-concept study strongly suggests that P2Y$_6$R antagonists may be beneficial for the treatment of obesity and T2D.

---

peripheral inflammation, suggesting that the lack of adipocyte $P2Y_6R$ is mainly responsible for this phenotype. Our data provide compelling evidence that attenuation of $P2Y_6R$ signaling in adipocytes can improve systemic glucose metabolism, suggesting that $P2Y_6R$ antagonists may be useful for the treatment of obesity and T2D.

Results

$P2Y_6R$ Is Expressed in Both Adipose Tissue and Skeletal Muscle and Is Regulated Differently in Diet-Induced Obese Mice.

To investigate the potential role of $P2Y_6R$ in energy homeostasis and glucose metabolism, we quantified the mRNA expression levels of $P2Y_6R$ in metabolically important tissues such as adipose tissue and skeletal muscle. Of the three major adipose depots, $P2Y_6R$ mRNA expression was significantly higher in epididymal WAT (eWAT, visceral fat) than in iWAT (subcutaneous [s.c.] fat) and BAT (Fig. 1A). Among the skeletal muscles examined, tibialis anterior (TA) muscle showed highest $P2Y_6R$ expression, followed by quadriceps (Q), gastrocnemius (G), and soleus (S) muscles (Fig. 1B).

Obesogenic diets affect the expression of various G protein-coupled receptors (GPCRs) in distinct tissues (21–23). Therefore, we hypothesized that expression of $P2Y_6R$ may be altered in adipose tissue and skeletal muscle during obesity. To test the hypothesis, adipose tissues were collected from C57BL/6 mice fed regular chow or a high-fat diet (HFD) for 8 wk, and skeletal muscle tissues were collected from mice fed chow diet (CD) or HFD for 16 wk. Interestingly, the HFD significantly increased $P2Y_6R$ mRNA expression in mature white adipocytes (free of immune cells) of iWAT and BAT (Fig. 1C). To our surprise, $P2Y_6R$ expression was decreased in TA and G skeletal muscle of mice fed on HFD (Fig. 1D), indicating a differential regulation of $P2Y_6R$ expression in the metabolic tissues under study.

Global Deletion of $P2Y_6R$ Protects Mice Against HFD-Induced Metabolic Deficits.

As we observed marked differences in $P2Y_6R$ expression in metabolic tissues of HFD mice, we aimed to investigate the effect of whole-body $P2Y_6R$ deletion (WB-$P2Y6^{\Delta/\Delta}$) on the development of obesity and systemic glucose homeostasis. As expected, $P2Y_6R$ mRNA was undetectable in multiple metabolic tissues of WB-$P2Y6^{\Delta/\Delta}$ mice, as compared to control mice (WB-$P2Y6^{WT/WT}$) (*SI Appendix*, Fig. S1A). A group of control and WB-$P2Y6^{\Delta/\Delta}$ mice (male C57BL/6 mice) was kept on HFD, and body weights were measured starting from 1 wk on HFD. Initially, WB-$P2Y6^{\Delta/\Delta}$ mice gained significantly less weight than control mice (Fig. 1E). Body weight gain on HFD was similar between the two groups (Fig. 1E). Liver weight was reduced, whereas iWAT weight was increased in HFD WB-$P2Y6^{\Delta/\Delta}$ mice, as compared to HFD control mice (*SI Appendix*, Fig. S1B). No difference was found in eWAT and BAT weights between the two groups (*SI Appendix*, Fig. S1B). Next, we subjected HFD WB-$P2Y6^{\Delta/\Delta}$ and control mice to a series of metabolic tests. Interestingly, WB-$P2Y6^{\Delta/\Delta}$ mice showed significant improvements in glucose tolerance and insulin sensitivity (Fig. 1 F and G). Improved glucose tolerance in WB-$P2Y6^{\Delta/\Delta}$ mice can be attributed to reduced body weight. No differences in blood glucose levels were observed between the two groups in a pyruvate challenge test, indicating that hepatic glucose output was similar in the two groups (*SI Appendix*, Fig. S1C). WB-$P2Y6^{\Delta/\Delta}$ mice exhibited reduced fasting blood glucose levels (Fig. 1H) and reduced plasma insulin levels under both fasting and fed conditions (Fig. 1I), indicating improved peripheral insulin sensitivity. Plasma free fatty acid (FFA) levels did not differ between the two mouse cohorts, indicating that $P2Y_6R$ does not play a significant role in adipose tissue lipolysis (*SI Appendix*, Fig. S1D). Deficiency of $P2Y_6R$ did not cause any significant changes in the expression of genes involved in adipocyte browning/mitochondrial function in iWAT and eWAT of WB-$P2Y6^{\Delta/\Delta}$, as compared to tissues from control littermates (*SI Appendix*, Fig. S1 E and F). Surprisingly, BAT lacking $P2Y_6R$ showed modest decreases in mRNA levels of genes such as *Ucp1*,

Pparα, and *Pparg* (*SI Appendix*, Fig. S1G). These observations were confirmed by UCP1 staining of iWAT, eWAT, and BAT sections of control and WB-$P2Y6^{\Delta/\Delta}$ mice (*SI Appendix*, Fig. S1H).

Reduced Inflammation in Global $P2Y_6R$-Deficient Mice.

Development of obesity and subsequent insulin resistance is associated with enhanced systemic inflammation (5, 24). Activation of $P2Y_6R$ by UDP has been shown to mediate inflammatory responses by increasing the secretion of proinflammatory cytokines such as monocyte chemoattractant protein-1 (MCP1) (16). Therefore, we hypothesized that global deletion of $P2Y_6R$ may protect mice from peripheral inflammation resulting from HFD consumption. To test this hypothesis, H&E and F4/80 staining was performed on iWAT and eWAT sections of HFD WB-$P2Y6^{\Delta/\Delta}$ and control mice. Imaging studies revealed an increased number of smaller adipocytes in both iWAT and eWAT of WB-$P2Y6^{\Delta/\Delta}$ compared to control tissues (Fig. 1 J and K). A similar phenomenon was observed with BAT sections (*SI Appendix*, Fig. S1I). eWAT sections from control mice with a functional $P2Y_6R$ exhibited crown-like structures indicating infiltration of inflammatory monocyte/macrophages. Such structures were reduced in eWAT sections of WB-$P2Y6^{\Delta/\Delta}$ mice (Fig. 1L). Similarly, iWAT sections also showed reduced infiltration of monocyte/macrophages in WB-$P2Y6^{\Delta/\Delta}$ mice (Fig. 1L). To further confirm these findings, mRNA levels of proinflammatory markers were quantified in different adipose depots. As expected, mRNA levels of macrophage markers (*F4/80* and *Cd68*) were significantly reduced in iWAT and eWAT of WB-$P2Y6^{\Delta/\Delta}$ mice (Fig. 1 M and N). Transcript levels of proinflammatory markers such as *Mcp1*, *Il6*, *Tnfα*, *Ifng*, *Mip1a*, and *Mip1b* were also significantly reduced in adipose depots of WB-$P2Y6^{\Delta/\Delta}$ mice (Fig. 1 M and N). In accordance with the gene expression data, circulating plasma levels of MCP1, resistin and IFNγ were significantly lower in WB-$P2Y6^{\Delta/\Delta}$ mice compared to control littermates (Fig. 1 O–R). Taken together, these data clearly indicate that global deletion of $P2Y_6R$ reduced peripheral inflammation thereby improving glucose homeostasis and insulin sensitivity.

Pharmacological Determination of Functional $P2Y_6R$ Expression in Mouse White and Brown Adipocytes.

We previously identified uracil nucleotide derivatives that act as potent human $P2Y_6R$ (h$P2Y_6R$) agonists (25). We selected the potent $P2Y_6R$ agonist MRS4383 (((1S,2R,3R,4S,5R)-3,4-dihydroxy-5-((Z)-4-(methoxyimino)-2-oxo-3,4-dihydropyrimidin-1(2H)-yl)bicyclo[3.1.0] hexan-2-yl)methyl diphosphate) to identify and demonstrate a functional $P2Y_6R$ expressed by mouse (m) adipocytes. Specifically, we first isolated the stromal vascular fraction (SVF) from both iWAT and BAT of WB-$P2Y6^{\Delta/\Delta}$ and control mice and then differentiated the cells into mature white or brown adipocytes. Treatment of mature adipocytes with different concentrations of MRS4383 resulted in accumulation of inositol monophosphate (IP1) in control cells expressing $P2Y_6R$ (Fig. 2 A and B). In contrast, this response was absent in cells lacking functional $P2Y_6R$ (Fig. 2 A and B). This experiment confirmed the specificity of MRS4383 for the G_q-coupled $P2Y_6R$ and the presence of functional $P2Y_6Rs$ in mouse white and brown adipocytes.

Generation of Adipocyte-Specific $P2Y_6R$ Knockout (KO) Mice (Adipo-$P2Y6^{\Delta/\Delta}$).

Given that global $P2Y_6R$ deletion improves glucose metabolism with reduced peripheral inflammation, we aimed to investigate whether abrogation of $P2Y_6R$ signaling in mature adipocytes affects energy and glucose homeostasis. To this end, we inactivated the $P2Y_6R$ gene selectively in mature adipocytes by crossing floxed $P2Y_6R$ (*P2Y6f/f*) mice with mice expressing Cre recombinase under the control of the adipocyte-specific adiponectin promoter (*adipoq-Cre* mice). This mating scheme gave rise to *P2Y6f/f* (control) and *adipoq-Cre^{+/−}P2Y6f/f* (adipo-$P2Y6^{\Delta/\Delta}$) mice. Real-time qPCR analysis revealed a significant knockdown of $P2Y_6R$ mRNA in mature adipocytes from
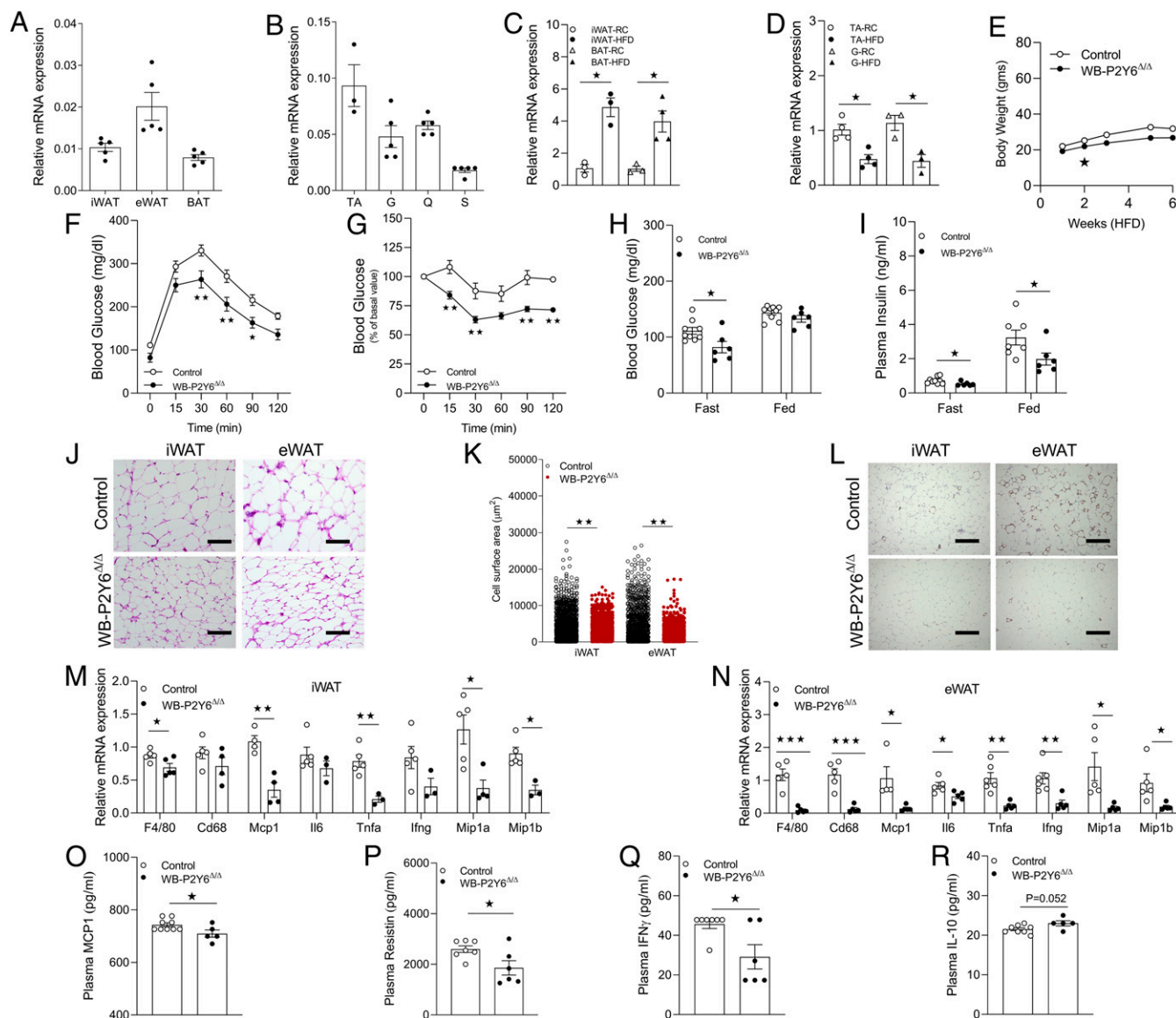
Fig. 1. Whole-body P2Y$_6$R KO mice (WB-P2Y6$^{\Delta/\Delta}$ mice) show reduced HFD-induced metabolic deficits and peripheral inflammation. (*A*) Relative expression of P2Y$_6$R mRNA in subcutaneous (s.c.) (iWAT), visceral (eWAT), and BAT (*n* = 5/group). (*B*) Relative expression of P2Y$_6$R-mRNA in tibialis anterior (TA), gastrocnemius (G), quadriceps (Q), and soleus (S) skeletal muscle (*n* = 3 to 5/group). (*C*) mRNA expression levels of P2Y$_6$R in iWAT (mature adipocytes) or BAT from regular chow (RC) or HFD-fed C57BL/6 control mice. (*n* = 3/group). (*D*) mRNA expression levels of P2Y$_6$R in TA or G from RC- or HFD-fed C57BL/6 control mice (*n* = 3 to 4/group). (*E*) Body weight (grams) of mice maintained on HFD for 6 wk (*n* = 5 to 6/group). (*F*) GTT (1 g/kg glucose, i.p.) (*n* = 6 to 9/group). (*G*) ITT (1 U/kg insulin, i.p.) (*n* = 5 to 9/group). (*H*) Fasting and fed blood glucose levels (*n* = 6 to 9/group). (*I*) Fasting and fed plasma insulin levels (*n* = 6 to 9/group). (*J*) Representative H&E-stained sections from iWAT and eWAT from WB-P2Y6$^{\Delta/\Delta}$ and control mice on HFD. (*K*) Quantification data of adipocytes area in iWAT and eWAT from WB-P2Y6$^{\Delta/\Delta}$ and control mice on HFD (*n* = 10 sections/group). (*L*) Representative F4/80-stained sections from iWAT and eWAT from WB-P2Y6$^{\Delta/\Delta}$ and control mice on HFD. (*M*) mRNA expression levels of inflammation markers in iWAT of WB-P2Y6$^{\Delta/\Delta}$ and control mice on HFD (*n* = 3 to 6/group). (*N*) mRNA expression levels of inflammation markers in eWAT of WB-P2Y6$^{\Delta/\Delta}$ and control mice on HFD (*n* = 3 to 6/group). (*O–R*) Circulating plasma levels of (*O*) MCP1, (*P*) resistin, (*Q*) IFNγ, and (*R*) IL-10 in WB- P2Y6$^{\Delta/\Delta}$ and control mice. (*n* = 5 to 9/group). The expression of 18s RNA was used to normalize qRT-PCR data. All data are expressed as means ± SEM. *$P < 0.05$, **$P < 0.01$, ***$P < 0.001$ (*C* and *D*, *H–R*: two-tailed Student's *t* test; *E–G*: two-way ANOVA followed by Bonferroni's post hoc test).

different adipose depots (iWAT, eWAT, and BAT) of adipo-P2Y6$^{\Delta/\Delta}$ mice (Fig. 2*C*). P2Y$_6$R expression remained unaltered in other metabolically active tissues (*SI Appendix*, Fig. S2*A*).

Adipo-P2Y6$^{\Delta/\Delta}$ Mice Are Protected from HFD-Induced Obesity and Metabolic Dysfunction. To assess the metabolic roles of adipocyte P2Y$_6$R, adipo-P2Y6$^{\Delta/\Delta}$ mice and control littermates were first maintained on regular chow diet. Under these conditions, the two groups of mice showed similar body weight, glucose tolerance, insulin sensitivity, blood glucose, plasma glycerol, FFA, and triglyceride levels

in either the fasting or fed state (*SI Appendix*, Fig. S2 *B–H*). However, under fasting conditions, plasma insulin levels were reduced in adipo-P2Y6$^{\Delta/\Delta}$ mice, while no difference was observed in the fed state (*SI Appendix*, Fig. S2*I*). Similarly, plasma leptin levels were reduced in adipo-P2Y6$^{\Delta/\Delta}$ mice (*SI Appendix*, Fig. S2*J*).

Next, to determine the potential role of adipocyte P2Y$_6$R in diet-induced dysregulation of energy homeostasis and glucose metabolism, adipo-P2Y6$^{\Delta/\Delta}$ and control mice were challenged with a HFD. Adipo-P2Y6$^{\Delta/\Delta}$ mice gained less body weight than control mice (Fig. 2*D*), and MRI scanning data revealed that

PHYSIOLOGY
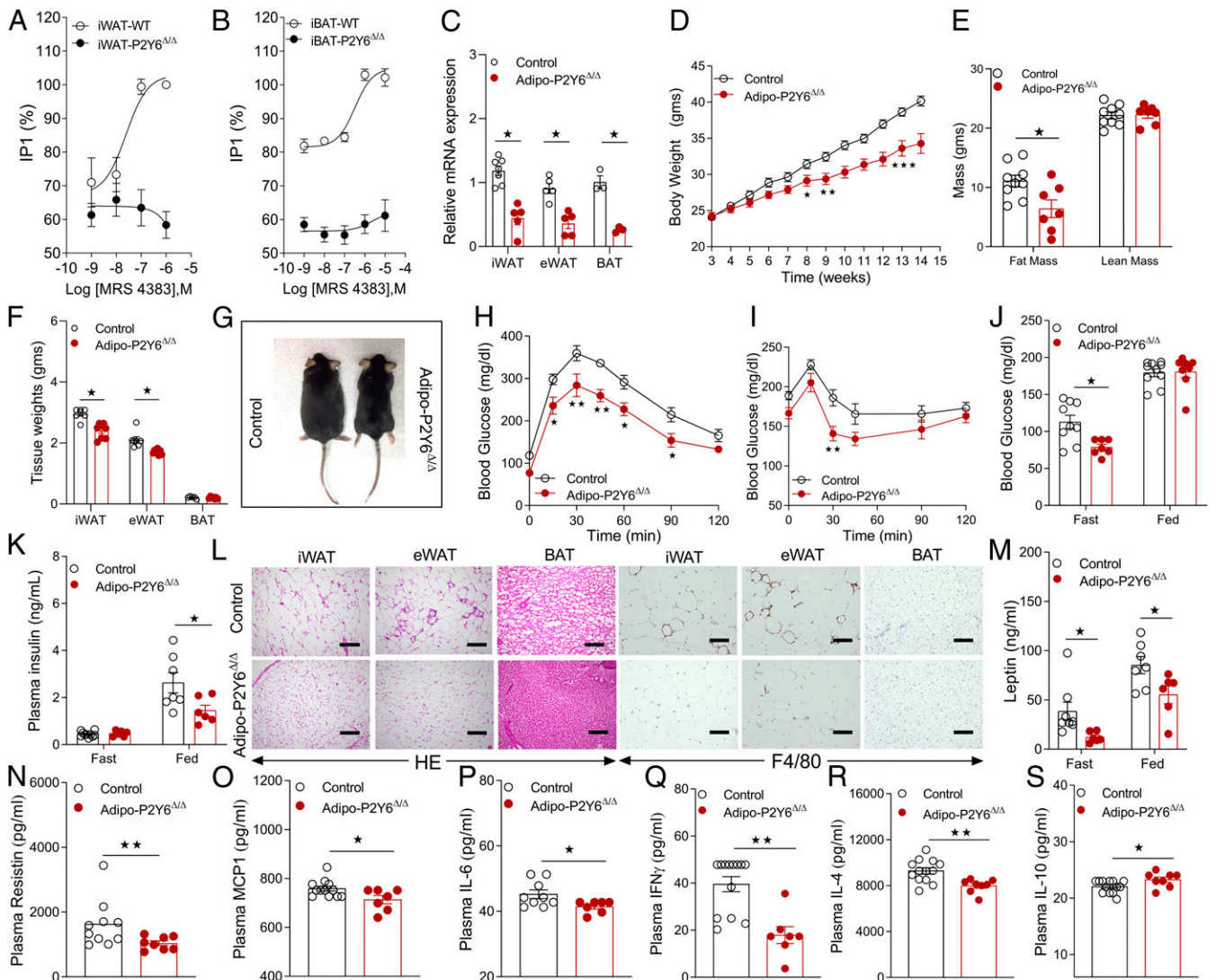
Fig. 2. Adipocyte-specific P2Y$_6$R KO mice (adipo-P2Y6$^{\Delta/\Delta}$ mice) are protected from HFD-induced obesity, metabolic deficits, and peripheral inflammation. (*A*) IP1 accumulation assay in the differentiated mature white adipocytes (iWAT) from WB-P2Y6$^{\Delta/\Delta}$ and control mice. (*n* = 3 to 4); each experiment was performed in triplicate. (*B*) IP1 accumulation assay in differentiated mature brown adipocytes from WB-P2Y6$^{\Delta/\Delta}$ and control mice (*n* = 3 to 4). Each experiment was performed in triplicate. (*C*) mRNA levels of P2Y$_6$R in mature adipocytes isolated from iWAT (*n* = 5 to 7/group), eWAT (*n* = 5/group), and BAT (*n* = 3/group) of adipo-P2Y6$^{\Delta/\Delta}$ and control mice. (*D*) Body weight measurements of mice maintained on HFD (*n* = 7 to 9/group). (*E*) Body composition (lean and fat mass in grams) of mice maintained on HFD (*n* = 7 to 9/group). (*F*) Tissue weights (iWAT, eWAT, and BAT) after 12 wk on HFD (*n* = 6 to 8/group). (*G*) Images of representative adipo-P2Y6$^{\Delta/\Delta}$ and control mice (10 wk on HFD). (*H*) GTT (1 g /kg glucose, i.p.) (*n* = 6–8/group). (*I*) ITT (1 U/kg insulin, i.p.) (*n* = 6 to 8/group). (*J*) Fasting and fed blood glucose levels (*n* = 7 to 10/group). (*K*) Fasting plasma insulin levels (*n* = 6 to 8/group). (*L*) Representative H&E- and F4/80-stained sections of iWAT, eWAT, and BAT from adipo-P2Y6$^{\Delta/\Delta}$ and control mice maintained on HFD. (*M–S*) Circulating plasma levels of (*M*) leptin, (*N*) resistin, (*O*) MCP1, (*P*) IL6, (*Q*) IFNγ, (*R*) IL4, and (*S*) IL10 in adipo-P2Y6$^{\Delta/\Delta}$ and control mice (*n* = 6 to 12/group). The expression of 18s RNA was used to normalize qRT-PCR data. All data are expressed as means ± SEM *P < 0.05, **P < 0.01 (*C–F, J–S*: two-tailed Student's *t* test; *H* and *I*: two-way ANOVA followed by Bonferroni's post hoc test). All experiments were conducted on mice fed on HFD.

differences in body weight were due to a significant reduction in fat mass in adipo-P2Y6$^{\Delta/\Delta}$ mice (Fig. 2 *E–G*). Next, a series of metabolic tests were carried out with both groups of mice maintained on HFD for 8 wk. Under these conditions, adipo-P2Y6$^{\Delta/\Delta}$ mice showed significant improvements in glucose tolerance (Fig. 2*H*) and insulin sensitivity (Fig. 2*I*). Moreover, blood glucose levels (fasting) and plasma insulin levels (fed) were significantly reduced in adipo-P2Y6$^{\Delta/\Delta}$ mice (Fig. 2 *J* and *K*). Loss of adipocyte P2Y$_6$R had no significant effect on adipocyte lipolysis as plasma FFA, glycerol, and total triglyceride levels were similar between the two groups (*SI Appendix*, Fig. S3 *A–C*).

To examine the effect of lack of P2Y$_6$R in adipocytes on whole-body energy homeostasis, we performed indirect calorimetry measurements (*SI Appendix*, Fig. S3). The measurements were performed on mice during the first week (first 4 d) of HFD feeding. Energy expenditure (EE) (kcal/day) was plotted against total body mass and analysis of covariance was applied to identify a potential difference in EE between the two groups (*SI Appendix*, Fig. S3*D*). ANCOVA analysis identified a significant difference in EE between the adipo-P2Y6$^{\Delta/\Delta}$ and control mice (*P* = 0.018) (*SI Appendix*, Fig. S3*D*). EE was reduced with increasing body mass in HFD control mice (negative correlation), and this phenomenon was absent in HFD adipo-P2Y6$^{\Delta/\Delta}$ mice (*SI Appendix*, Fig. S3*D*). Enhanced EE in adipo-P2Y6$^{\Delta/\Delta}$ mice

may result in reduced obesity over a long period of HFD feeding. No significant difference in food intake (*SI Appendix*, Fig. S3*E*) and oxygen consumption rate (*SI Appendix*, Fig. S3*F*) was observed between adipo-P2Y6$^{\Delta/\Delta}$ and control mice. However, the respiratory exchange ratio (RER) tended to be reduced ($P = 0.08$) in adipo-P2Y6$^{\Delta/\Delta}$ mice (*SI Appendix*, Fig. S3*G*). Reduced RER points toward increased lipid oxidation in adipocytes of adipo-P2Y6$^{\Delta/\Delta}$ mice and may contribute to reduced adiposity.

Adipo-P2Y6$^{\Delta/\Delta}$ Mice Showed Reduced Inflammation on HFD. As global deletion of P2Y$_6$R ameliorates inflammation associated with HFD feeding, we investigated whether deletion of P2Y$_6$R specifically in mature adipocytes affected peripheral inflammation. To test this hypothesis, H&E and F4/80 stained iWAT, eWAT, and BAT sections from HFD adipo-P2Y6$^{\Delta/\Delta}$ and control mice were analyzed microscopically. Adipose tissue (eWAT) from control mice showed pronounced infiltration of proinflammatory immune cells (Fig. 2*L*). This effect was significantly reduced in eWAT of HFD adipo-P2Y6$^{\Delta/\Delta}$ mice (Fig. 2*L*). Consistent with the results obtained with WB-P2Y6$^{\Delta/\Delta}$ mice, adipo-P2Y6$^{\Delta/\Delta}$ mice also showed significantly smaller adipocyte size, as compared to the corresponding adipose tissues from control littermates (Fig. 2*L*).

Under conditions of obesity and T2D, the secretion of adipokines/cytokines from adipocytes changes drastically, resulting in significant effects on whole body glucose and energy metabolism (6, 26). P2Y$_6$R has been shown to regulate the secretion of cytokines mediating inflammation under pathophysiological conditions (27). Therefore, we measured circulating levels of adipokines/cytokines in adipo-P2Y6$^{\Delta/\Delta}$ mice. Plasma leptin and resistin levels were reduced in adipo-P2Y6$^{\Delta/\Delta}$ mice, consistent with reduced obesity (Fig. 2 *M* and *N*). Among the proinflammatory cytokines, plasma levels of MCP1, IL6, IFNγ, and IL4 were significantly decreased, while the levels of IL10, an antiinflammatory cytokine, were increased in adipo-P2Y6$^{\Delta/\Delta}$ mice (Fig. 2 *O–S*). Consistent with staining data, mRNA expression levels of macrophage markers (*F4/80* and *Cd68*) were significantly reduced in iWAT, eWAT, and BAT from adipo-P2Y6$^{\Delta/\Delta}$ mice (*SI Appendix*, Fig. S3 *I–K*). In agreement with the plasma cytokine levels, iWAT showed decreased transcript levels of *Mcp1*, *Ifng*, and *Il6*, while eWAT displayed reduced gene expression of *Mip1a*, *Mip1b*, and *Tnfa* (*SI Appendix*, Fig. S3 *I and J*).

Collectively, these experiments revealed that either global deletion or adipocyte-specific deficiency of P2Y$_6$R protects against obesity-associated inflammation and improves glucose and insulin tolerance in mice.

Reduced Hepatic Steatosis and Hepatic Inflammation in Adipo-P2Y6$^{\Delta/\Delta}$ Mice. Since adipo-P2Y6$^{\Delta/\Delta}$ mice showed reduced adiposity but no change in plasma FFA levels, we aimed to understand the effect of reduced fat mass on the ectopic deposition of fat in tissues like liver. Liver sections from HFD adipo-P2Y6$^{\Delta/\Delta}$ and control mice were subjected to hematoxylin and eosin (H&E) and Oil Red O (ORO) staining. Microscopic analysis revealed reduced deposition of fat in the liver of adipo-P2Y6$^{\Delta/\Delta}$ mice (*SI Appendix*, Fig. S4*A*). Consistent with the observation, liver weight as well as liver triglyceride levels were decreased in the adipo-P2Y6$^{\Delta/\Delta}$ mice (*SI Appendix*, Fig. S4 *B and C*). The decrease in fat deposition resulted in reduced hepatic inflammation as evident from the reduced mRNA levels of inflammatory markers (*Il6*, *Ifng*, *Mcp1*, *Mip1b*, and *Il1b*) in the liver of adipo-P2Y6$^{\Delta/\Delta}$ mice, contributing to reduced peripheral inflammation (*SI Appendix*, Fig. S4*D*). However, no significant differences in expression levels of genes involved in the hepatic glucose and lipid metabolism were observed (*SI Appendix*, Fig. S4*E*).

P2Y$_6$R-Mediated JNK Activation in Mature White Adipocytes. G$_q$ protein-dependent activation of JNK signaling has been reported previously (28). JNK activation in adipocytes has been shown to result in metabolic dysfunction (29). Hence, we hypothesized that

P2Y$_6$R-mediated signaling may affect JNK activation in adipocytes and contribute to the observed metabolic phenotype. To this end, preadipocytes from iWAT of WB-P2Y6$^{\Delta/\Delta}$ and control mice were isolated and differentiated into mature adipocytes. Mature adipocytes were stimulated with the P2Y$_6$R-selective agonist MRS4383 for specific periods of time, and JNK phosphorylation was quantified. Strikingly, P2Y$_6$R activation caused phosphorylation of JNK in control adipocytes but not in WB-P2Y6$^{\Delta/\Delta}$-derived adipocytes (Fig. 3*A*). Adipocytes lacking P2Y$_6$R also showed decreased levels of p-cJUN, a downstream effector of JNK (Fig. 3*B*). We also quantitated protein levels of total JNK (T-JNK) and p-JNK in iWAT from adipo-P2Y6$^{\Delta/\Delta}$ and control mice. Strikingly, iWAT from adipo-P2Y6$^{\Delta/\Delta}$ mice showed decreased levels of T-JNK and p-JNK compared to control mice (Fig. 3 *C* and *D*), confirming our hypothesis that activation of P2Y$_6$R regulates JNK and cJUN.

P2Y$_6$R Regulates the JNK-PPARα-PGC1α Axis in White Adipocytes. To further delineate the contribution of P2Y$_6$R-mediated JNK signaling in the regulation of adipocyte metabolism, we identified a signaling cascade downstream of P2Y$_6$R in adipocytes. In cardiac myocytes, transcription of PPARα is regulated by binding of cJUN to the PPARα promoter region (30). Since P2Y$_6$R activation regulates JNK, we investigated whether JNK-mediated activation of cJUN affected the expression of PPARα. To this end, we performed a chromatin immunoprecipitation (ChIP) assay using nuclear DNA from adipocytes expressing P2Y$_6$R with or without stimulation with P2Y$_6$R agonist (MRS4383, 1 μM). P2Y$_6$R activation led to an increase in the enrichment of PPARα promoter sequence in DNA isolated from cJUN antibody-bound chromatin regions (Fig. 3 *E* and *F*). To further demonstrate that P2Y$_6$R-mediated JNK activation can regulate PPARα, we treated cultured mature adipocytes from WB-P2Y6$^{\Delta/\Delta}$ and control mice with JNK inhibitor (SP600125, 25 μM) and then stimulated with P2Y$_6$R agonist (MRS4383, 1 μM) for the indicated time period. Treatment of cells with the JNK inhibitor alone had no effect on *Ppara* mRNA levels in adipocytes (Fig. 3*G*). However, treatment of cells with P2Y$_6$R agonist decreased *Ppara* mRNA levels in control cells but not in adipocytes lacking P2Y$_6$R expression, indicating P2Y$_6$R-specific regulation of *Ppara* levels (Fig. 3*G*). The observed decrease in *Ppara* levels by P2Y$_6$R activation could be prevented by pretreatment of cells with JNK inhibitor (Fig. 3*G*). P2Y$_6$R activation in adipocytes also decreased *PGC1α* mRNA levels, a coactivator of PPARα in the transcriptional control of mitochondrial genes (Fig. 3*H*). Consistent with the change in mRNA levels, the level of PGC1α and PPARα proteins were significantly decreased after P2Y$_6$R activation (Fig. 3*I*). Prior treatment of adipocytes with JNK inhibitor rescued the decrease in PGC1α and PPARα protein levels due to P2Y$_6$R activation (Fig. 3*I*). Taken together, our data indicate that JNK-mediated cJUN activation promotes the cJUN interaction with the PPARα promoter, regulating the expression of PPARα and its downstream target and coactivator such as PGC1α.

Further, we examined PPARα activity following P2Y$_6$R activation using a luciferase reporter assay. PPARα forms a heterodimer with the retinoid X receptor (RXR) that binds to their DNA binding element known as PPAR response element (PPRE)/Direct repeat 1 (DR1) (31). Astrocytoma 1321N1 cells expressing hP2Y$_6$R were transiently transfected with DR1 plasmid with or without plasmids expressing PPARα/RXR. Stimulation of transfected cells with MRS4383 (1 μM) decreased the luciferase activity, indicating that decreased PPARα activity was due to activation of P2Y$_6$R signaling in these cells (Fig. 3*J*).

Ablation of P2Y$_6$R in iWAT Promotes the Expression of Mitochondrial/ Beiging-Specific Genes. To recapitulate the effects of P2Y$_6$R signaling observed in primary adipocytes, whole-transcriptome analysis of iWAT from HFD adipo-P2Y6$^{\Delta/\Delta}$ and control mice was performed. Analysis of differentially expressed genes revealed
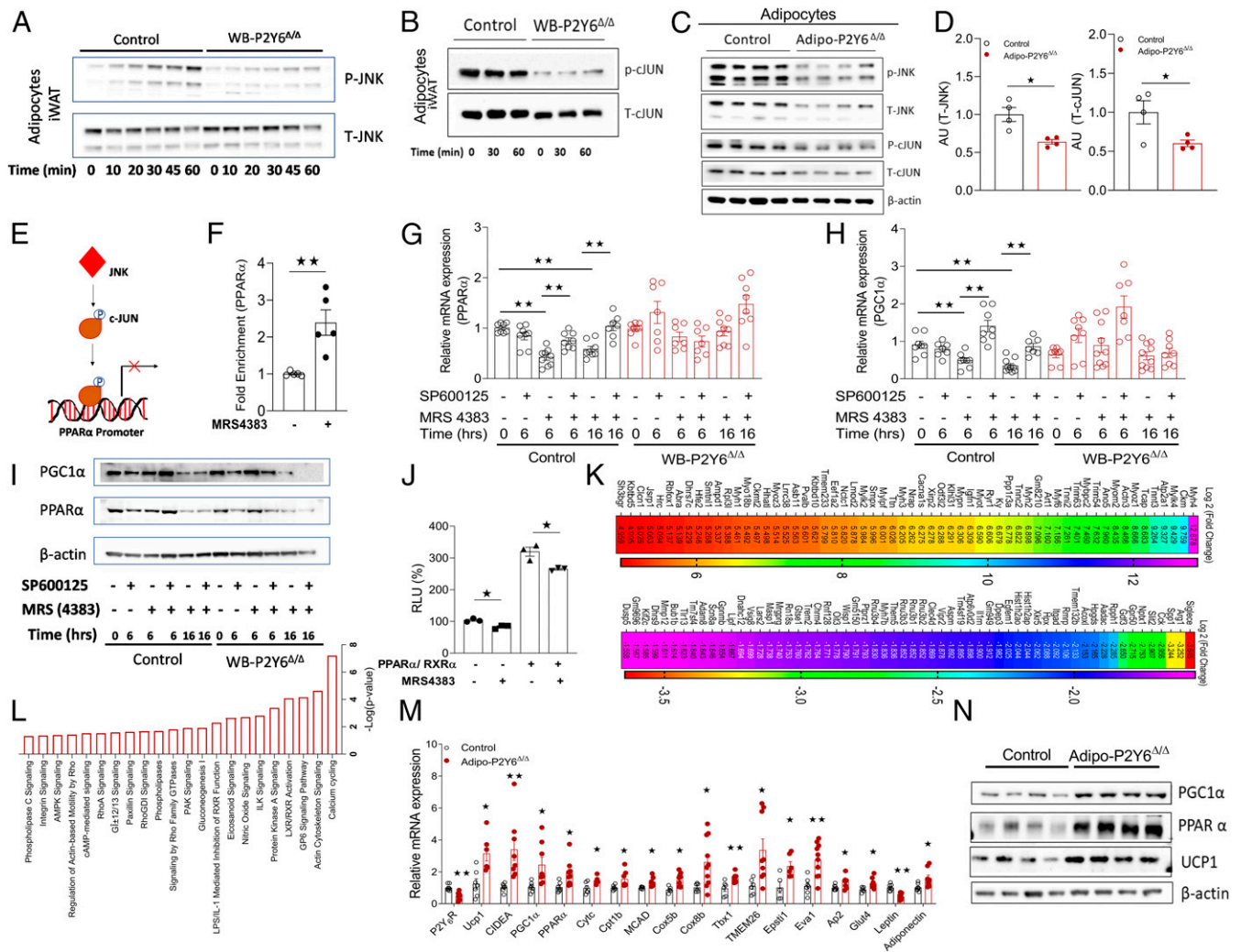
Fig. 3. P2Y$_6$R regulates JNK-PPARα-PGC1α axis in white adipocytes. (*A* and *B*) Western blot analysis of (*A*) p-JNK/T-JNK and (*B*) p-cJUN/T-cJUN protein expression in mature adipocytes differentiated from iWAT preadipocytes isolated from WB-P2Y6$^{Δ/Δ}$ and control mice. Mature adipocytes were treated with P2Y$_6$R agonist, MRS4383 (1 μM), and cells were collected at the indicated time points. Representative blots are shown (*n* = 3 to 4 independent experiments). (*C*) Western blots showing increased T-JNK, p-JNK, T-cJUN, and p-cJUN expression in iWAT of HFD-fed adipo-P2Y6$^{Δ/Δ}$ and control mice. Each lane represents a different mouse (*n* = 4/group). (*D*) Quantification of immunoblotting data shown in *C*. (*E*) Schematic representation of the mechanism by which P2Y$_6$R activation regulates the interaction between cJUN and the *PPARα* promoter. (*F*) Chip assay showing fold enrichment of *PPARα* promoter region in mature adipocytes differentiated from iWAT preadipocytes isolated from WT mice. Mature adipocytes were treated with P2Y$_6$R agonist, MRS4383 (1 μM) and cells were collected after 2.5 h. (*n* = 5 independent experiments). (*G* and *H*) mRNA expression analysis of (*G*) *Ppara* and (*H*) *Pgc1a* genes in differentiated iWAT adipocytes isolated from WB-P2Y6$^{Δ/Δ}$ and control mice. Mature adipocytes were incubated with JNK inhibitor (SP600126, 25 μM) and/or P2Y$_6$R agonist (MRS4383, 1 μM) for the indicated periods of time. Cells were collected at specific time points as indicated (*n* = 7 to 9/group). (*I*) Western blot analysis for PGC1α and PPARα protein expression in differentiated iWAT adipocytes isolated from WB-P2Y6$^{Δ/Δ}$ and control mice. The cells were treated in the same manner as in *G* and *H*. A representative blot is shown (*n* = 3 independent experiments). (*J*) PPARα activity assay using a luciferase assay in 1321N1 astrocytoma cells expressing human (h) P2Y$_6$R. Transfected cells were treated with MRS4383, 1 μM for 6 h. Relative luciferase activity was normalized to β-galactosidase activity for each sample (*n* = 3 independent experiments). (*K*) RNA-seq analysis showing the 60 top up-regulated and 60 top down-regulated genes in iWAT of HFD adipo-P2Y6$^{Δ/Δ}$ compared to HFD control littermates. Data are represented as a heat map of genes where color gradation corresponds to the log2 (fold change) (*n* = 6 libraries/group). (*L*) Column representation of significantly regulated pathways for all differentially expressed genes in iWAT of adipo-P2Y6$^{Δ/Δ}$ mice (*P* < 0.05, ingenuity pathway analysis [IPA]) (*n* = 6 libraries/group). (*M*) RT-PCR for verifying changes in mRNA expression of browning/mitochondrial markers in iWAT of adipo-P2Y6$^{Δ/Δ}$ mice compared to the control group (*n* = 4 to 6 per group). (*N*) Western botting analysis of PGC1α, PPARα, and UCP1 protein levels in iWAT of adipo-P2Y6$^{Δ/Δ}$ and control mice (*n* = 4/group). The expression of 18s RNA was used to normalize qRT-PCR data. All data are expressed as means ± SEM. *P* < 0.05, **P* < 0.01 (two-tailed Student's *t* test). RLU, relative luminescence units. All preadipocytes were isolated from RC-fed mice. Preadipocytes were differentiated to mature adipocytes for experiments.

that ∼406 genes were up-regulated, whereas ∼470 genes were down-regulated in iWAT of adipo-P2Y6$^{Δ/Δ}$ mice (Genomatix Genome Analyzer, cutoff: log2 (fold change) ≥ 0.58, *P* value 0.05) (Fig. 3*K* and *SI Appendix*, Table S1). G$_q$ protein-mediated pathways such as cellular calcium fluxes and actin-cytoskeletal signaling were found regulated in the iWAT of adipo-P2Y6$^{Δ/Δ}$ mice (Fig. 3*L*).

Lack of P2Y$_6$R resulted in up-regulation of transcript levels coding for *Ppara* and *Pgc1a* in iWAT of adipo-P2Y6$^{Δ/Δ}$ mice (Fig. 3*M* and *SI Appendix*, Fig. S5*A*), similar to the effects observed in primary adipocytes lacking P2Y$_6$R. Genes involved in mitochondrial function/brown adipocyte function (*Ucp1*, *Ucp3*, *Pgc1b*, *Evovl6*, *Cox8b*, *Cytc*, etc.) were up-regulated in iWAT of adipo-P2Y6$^{Δ/Δ}$, resulting in a switch of white adipocytes to brown adipocyte-like

cells (Fig. 3M and *SI Appendix*, Fig. S5A). Consistent with the gene expression data, protein levels of UCP1, PPARα, and PGC1α were dramatically increased in iWAT of adipo-P2Y6$^{\Delta/\Delta}$ mice (Fig. 3N). UCP1 staining revealed emergence of small brown like adipocytes in iWAT of adipo-P2Y6$^{\Delta/\Delta}$ mice (*SI Appendix*, Fig. S5B). In addition, mitochondrial DNA copy number was also significantly increased in iWAT of adipo-P2Y6$^{\Delta/\Delta}$ mice, consistent with the higher expression of PGC1α, a master regulator of mitochondrial biogenesis (*SI Appendix*, Fig. S5C). In agreement with this observation, the expression of genes coding for mitochondrial transcription factors such as *Nrf1* and *Tfam* and other mitochondrial genes (*Mtco1* and *Mtco2*) were also up-regulated in iWAT of adipo-P2Y6$^{\Delta/\Delta}$ mice (*SI Appendix*, Fig. S5D).

Taken together, these experiments demonstrate that white adipocytes lacking P2Y$_6$R show reduced JNK signaling, resulting in enhanced PPARα-PGC1a activity, up-regulation of mitochondrial biogenesis, and mitochondria-specific gene expression imparting a beige-like phenotype to white adipocytes, thereby contributing to reduced inflammation and improved metabolism.

We also carried out transcriptome analysis using total RNA isolated from BAT of adipo-P2Y6$^{\Delta/\Delta}$ and control mice. The expression levels of genes important for brown adipose function were not significantly different between adipo-P2Y6$^{\Delta/\Delta}$ and control mice. A list of genes differentially expressed between the groups is given in *SI Appendix*, Table S2.

Generation and Metabolic Analysis of Skeletal Muscle-Specific P2Y$_6$R KO Mice (SM-P2Y6$^{\Delta/\Delta}$ Mice). Having shown that global and adipocyte-specific deletion of P2Y$_6$R improves glucose homeostasis, we hypothesized that deletion of P2Y$_6$R in skeletal muscle, an important tissue for maintaining glucose homeostasis, may also affect the glucose metabolism. To address this issue, we generated mice lacking P2Y$_6$R selectively in skeletal muscle (SM-P2Y6$^{\Delta/\Delta}$) by crossing P2Y$_6$R-floxed mice with mice constitutively expressing the *HSA-Cre* transgene. Expression of HSA-Cre resulted in knockdown of P2Y$_6$R mRNA selectively in skeletal muscles (*SI Appendix*, Fig. S6A). Expression of P2Y$_6$R mRNA remained unaltered in other major metabolically active tissues (*SI Appendix*, Fig. S6B).

SM-P2Y6$^{\Delta/\Delta}$ mice and control littermates maintained on chow diet showed no significant differences in body weight, glucose tolerance, insulin sensitivity, or blood glucose and plasma insulin levels (*SI Appendix*, Fig. S6 C–G). Next, to determine the effect of SM-specific P2Y$_6$R deletion on HFD-induced metabolic deficits, we kept mice on HFD starting at 4 wk of age. SM-P2Y6$^{\Delta/\Delta}$ mice gained similar weight compared to control mice on HFD for 8 wk (Fig. 4A). HFD SM-P2Y6$^{\Delta/\Delta}$ mice displayed significantly impaired glucose tolerance and insulin sensitivity compared to control mice (Fig. 4 B and C). Consistent with these metabolic deficits, fasting and fed blood glucose as well as plasma insulin levels were increased in SM-P2Y6$^{\Delta/\Delta}$ mice (Fig. 4 D and E). Somewhat surprisingly, lack of P2Y$_6$R in skeletal muscle did not change circulating levels of myokines (*SI Appendix*, Fig. S6 H–L). We also studied expression levels of skeletal muscle myofiber markers to examine a potential switch from oxidative to glycolytic myofibers or vice versa. The expression of *Myh4*, a marker for type 2b nonoxidative myofibers, was unchanged in skeletal muscle of WB-P2Y6$^{\Delta/\Delta}$ and SM-P2Y6$^{\Delta/\Delta}$ mice, as compared to their respective control groups (Fig. 4 F and G). The mRNA expression levels of *Myh2* and *Myh7*, markers for type 1 and type 2a oxidative myofibers, were decreased in muscle lacking P2Y$_6$R (Fig. 4 F and G). Further, the expression levels of genes related to mitochondrial function/oxidative phosphorylation were decreased in muscle of SM-P2Y6$^{\Delta/\Delta}$ mice (Fig. 4H). Decreases in oxidative fibers were reported in individuals with obesity or T2D (32, 33). Our data suggest that a decrease in oxidative fibers in skeletal muscle of mice lacking P2Y$_6$R may contribute to impaired glucose homeostasis.

Activation of P2Y$_6$R Enhances Glucose Uptake in Skeletal Muscle. Since mice lacking P2Y$_6$R in skeletal muscle showed significant metabolic deficits, we hypothesized that P2Y$_6$R may play a role in glucose uptake in skeletal muscle. To test this, differentiated C2C12 myotubes were stimulated with P2Y$_6$R agonist MRS4383 (1 μM). P2Y$_6$R activation led to a significant increase in the uptake of radiolabeled 2-deoxyglucose (2-DG). Treatment of cells with P2Y$_6$R antagonist MRS2578 (1 μM) prior to stimulation with P2Y$_6$R agonist blocked 2-DG uptake by the myotubes (Fig. 4I). We next overexpressed P2Y$_6$R in C2C12 myotubes using an adenovirus coding for P2Y$_6$R. Cells transduced with a GFP-coding adenovirus were studied for control purposes. Cells overexpressing P2Y$_6$R showed enhanced 2-DG uptake compared to the control cells when treated with P2Y$_6$R agonist (Fig. 4J).

Next, we studied insulin-stimulated in vivo glucose uptake in SM-P2Y6$^{\Delta/\Delta}$ and control mice maintained on HFD for 20 wk. As predicted, insulin-mediated glucose uptake in skeletal muscle was significantly lower in SM-P2Y6$^{\Delta/\Delta}$ mice than in control littermates (Fig. 4K). No difference in insulin-mediated glucose uptake was found in iWAT, BAT, liver, and heart of SM-P2Y6$^{\Delta/\Delta}$ and control mice (Fig. 4 L and M and *SI Appendix*, Fig. S6 M–O). These data suggest that activation of P2Y$_6$R increases glucose uptake in skeletal muscle independent of the insulin response. In addition, lack of P2Y$_6$R in vivo renders skeletal muscle resistant to insulin-mediated glucose uptake, thus contributing to impaired glucose homeostasis.

Discussion

Obesity and T2D are major health problems worldwide. GPCRs have emerged as major drug targets for various diseases, including obesity and T2D (34–36). GPCRs are key players in the control of glucose and energy metabolism, and their function is regulated by various metabolites, neurotransmitters, hormones, and nucleotides. Nucleotides and their derivatives activate the P2Y GPCR subfamily. Plasma and tissue levels of these nucleotides fluctuate with energy state and regulate various cell processes through P2YRs and other purinergic receptors (11). In the current study, we systematically analyzed the functional role of P2Y$_6$R by making global, adipocyte-specific, and skeletal muscle-specific KO mice. We demonstrated that loss of P2Y$_6$R in mature adipocytes profoundly improved their function in WAT by inducing "beiging" and inhibiting JNK signaling. These changes led to improved systemic glucose metabolism and significantly reduced inflammation. Surprisingly, skeletal muscle P2Y$_6$R deletion impaired glucose homeostasis, due to decreased nucleotide-mediated glucose uptake. Moreover, we found that global lack of P2Y$_6$R improved glucose homeostasis, suggesting a dominant contribution by adipose tissue P2Y$_6$R to the improved systemic glucose metabolism.

P2Y$_6$R is expressed in various cell types, and its expression is enhanced by inflammatory stimuli or tissue injury (37–39). Feeding mice an obesogenic diet increased P2Y$_6$R expression in mature adipocytes, reflecting the receptor's role in adipocyte-associated pathophysiology in the development of obesity and related metabolic disorders. Here, we show that genetic deletion of P2Y$_6$R from mature adipocytes prevented adipocyte hypertrophy and improved glucose tolerance and insulin sensitivity in obese mice. The robust phenotype in adipo-P2Y6$^{\Delta/\Delta}$ mice was evident in the reduced expression of proinflammatory cytokines and lower plasma cytokine levels, suggesting that P2Y$_6$R activation causes obesity-associated inflammation in adipose tissue.

We also demonstrated that P2Y$_6$R deletion resulted in profound molecular changes in WAT. These changes were associated with enhanced beiging of WAT with increased expression of genes involved in mitochondrial function/brown adipocyte function (*Ucp1*, *Ucp3*, *Pgc1a*, *Pgc1b*, *Ppara*, etc). In agreement with the enhanced expression of PGC1α, a master regulator of
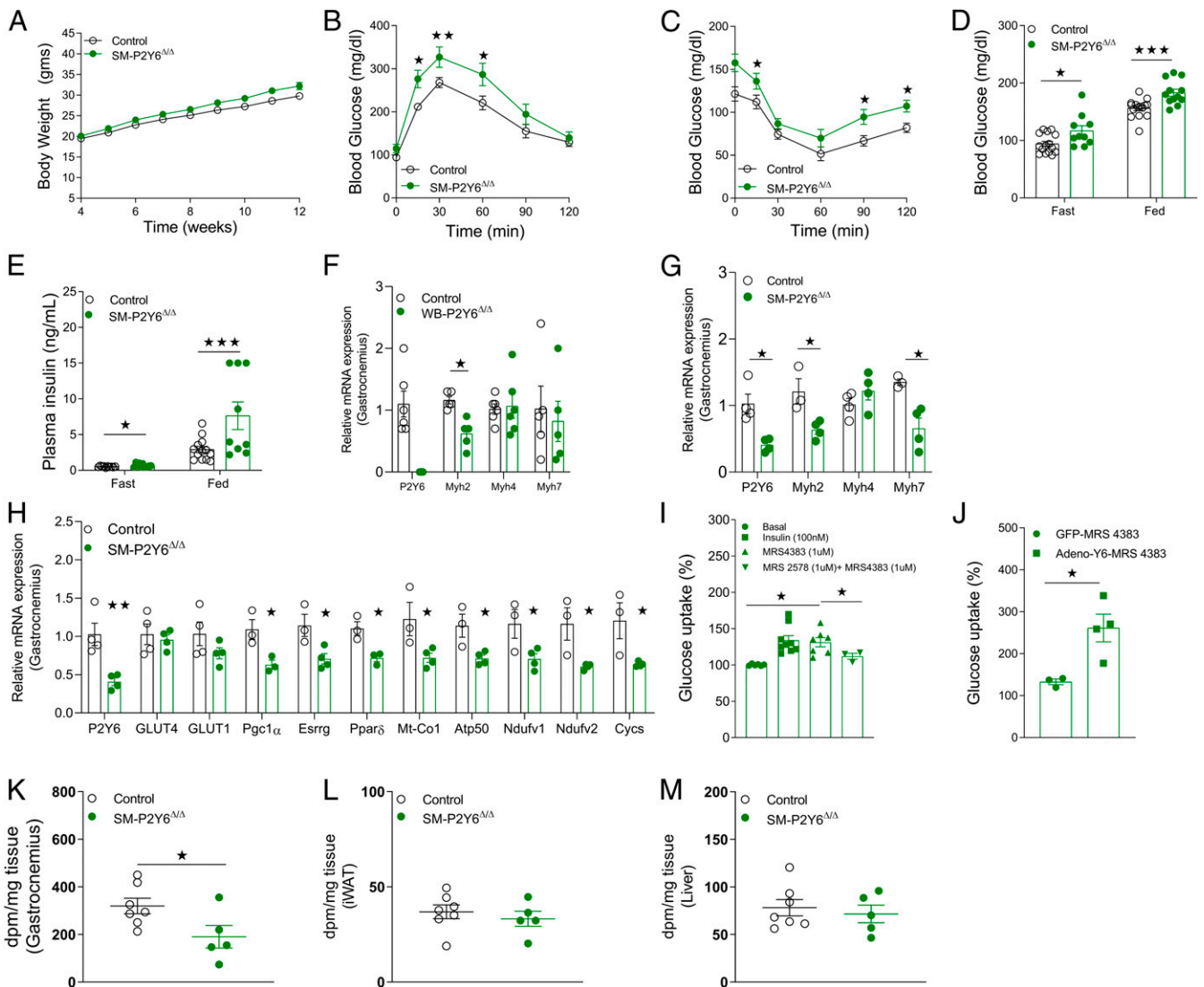
Fig. 4. Mice with P2Y$_6$R knockout in skeletal muscle (SM-P2Y6$^{\Delta/\Delta}$ mice) show greater impairments in glucose homeostasis when maintained on HFD. (*A*) Body weight measurements of mice maintained on HFD ($n = 9$ to 13/group). (*B*) GTT (1 g /kg glucose, i.p.) ($n = 9$ to 13/group). (*C*) ITT (1 U/kg insulin, i.p.) ($n = 9$ to 13/group). (*D*) Fasting and fed blood glucose levels ($n = 9$ to 13/group). (*E*) Fasting and fed plasma insulin levels ($n = 9$ to 13/group). (*F*) mRNA levels of P2Y$_6$R and markers of myofiber types in gastrocnemius muscle isolated from WB-P2Y6$^{\Delta/\Delta}$ and control mice fed with HFD for 16 wk ($n = 5$ to 6/group). (*G*) Quantifying mRNA levels of markers of myofiber types and P2Y$_6$R in gastrocnemius muscle isolated from SM-P2Y6$^{\Delta/\Delta}$ and control mice fed with HFD for 20 wk ($n = 3$ to 4/ group). (*H*) mRNA levels of mitochondrial/oxidative phosphorylation markers in gastrocnemius muscle isolated from SM-P2Y6$^{\Delta/\Delta}$ and control mice maintained on HFD for 20 wk ($n = 3$ to 4/group). (*I*) Glucose uptake (%) in C2C12 skeletal muscle cells after treatment with insulin (100 nM), P2Y$_6$R agonist (MRS4383, 1 µM) with or without P2Y$_6$R antagonist (MRS2578, 1 µM). ($n = 3$ independent experiments). (*J*) Glucose uptake (%) in C2C12 skeletal muscle cells transduced with adenovirus expressing GFP or mouse P2Y$_6$R. Cells were treated with P2Y$_6$R agonist (MRS4383, 1 µM) before quantifying glucose uptake ($n = 4$ independent experiments). (*K*–*M*) In vivo ^{14}C-2-deoxy-glucose uptake. SM-P2Y6$^{\Delta/\Delta}$ and control mice fed with HFD for 20 wk were injected with insulin (Humulin, 0.75 U/kg, i.p.) and a trace amount of [1-^{14}C]2-deoxy-D-glucose (10 µCi). After 40 min, mice were killed, and tissues were collected. Quantification of glucose uptake in (*K*) gastrocnemius, (*L*) IWAT, and (*M*) liver tissue ($n = 5$ to 7/group). The expression of 18s RNA was used to normalize qRT-PCR data. All data are expressed as means ± SEM. *$P < 0.05$, **$P < 0.01$, ***$P < 0.001$ (*A* and *D*–*M*: two-tailed Student's *t* test; *B* and *C*: two-way ANOVA followed by Bonferroni's post hoc test).

mitochondrial biogenesis, mitochondrial number was increased in WAT of adipo-P2Y6$^{\Delta/\Delta}$ mice. This observation supports previous data obtained via designer receptor exclusively activated by designer drugs (DREADD) technology, showing that G$_q$ activation results in reduced "browning" of WAT (40). Another interesting observation was the enhanced expression of sarcoplasmic/endoplasmic reticulum Ca^{2+}-ATPase1 (SERCA1-encoded by *Atp2a1*) and ryanodine receptor 1 (*Ryr1*) in WAT of adipo-P2Y6$^{\Delta/\Delta}$ mice. These proteins are highly expressed in BAT and are involved in calcium cycling between cytosol and the endoplasmic reticulum, releasing energy from ATP hydrolysis in

the form of heat (41). A previous study reported the role of Serca2 and Ryr2 in UCP1-independent thermogenesis in beige adipose tissue (42). Interestingly, no changes in Serca2 expression were observed in our study in WAT of adipo-P2Y6$^{\Delta/\Delta}$ mice. These findings suggest that lack of P2Y$_6$R might lead to Serca isoform-selective calcium cycling in adipocytes. More detailed studies will be required to investigate the possible contribution of P2Y$_6$R-mediated regulation of Serca1 expression to thermogenesis in adipocytes. Surprisingly, knockdown of P2Y$_6$R in brown adipocytes did not alter the expression of genes involved in brown adipogenesis or thermogenesis. Indirect calorimetry

analysis revealed that enhanced EE contributes to reduced body weight of adipo-P2Y6$^{\Delta/\Delta}$ mice over a long period of HFD feeding. Further, a trend ($P = 0.08$) toward reduced RER was observed in adipo-P2Y6$^{\Delta/\Delta}$ mice, indicative of enhanced lipid oxidation in adipocytes that may contribute to reduced adiposity.

Native agonist (UDP)-mediated activation of P2Y$_6$R results in IP$_3$ accumulation and an increase in cytoplasmic Ca^{2+} levels (43). Maintenance of Ca^{2+} homeostasis is essential for the functioning of most metabolic organs, including skeletal muscle, pancreas, and heart (44–46). In adipocytes, alterations in calcium signaling play a major role in the development of metabolic disorder. Rise in cytosolic Ca^{2+} in adipocytes has been shown to promote triglyceride accumulation, reduce lipolysis, inhibit early stages of murine adipocyte differentiation, and promote the production of inflammatory cytokines and immune mediators (47–49). Furthermore, older hypertensive, obese patients show elevated cytosolic Ca^{2+} levels in adipocytes (50). In tissues such as liver, increased cytosolic Ca^{2+} levels contribute to JNK activation, inflammatory signaling, and enhanced glucose production (51). Also, in obesity, JNK activity increases significantly in adipose tissue, resulting in severe metabolic impairments (29). Mice lacking JNK proteins are resistant to diet-induced obesity, steatosis, inflammation, and insulin resistance (52, 53). A study by Zhang et al. aimed to define the role of JNK activation in the adipose tissue in the development of obesity and associated deficits (54). Transgenic mice overexpressing dominant-negative JNK specifically in adipose tissue showed reduced weight gain, fat mass, and size of adipocytes. The transgenic mice were also resistant to HFD-induced insulin resistance, glucose intolerance, and hepatic steatosis, showed reduced inflammation and macrophage infiltration in adipose tissue and enhanced energy expenditure (54). Taken together, these studies strongly suggest that reduced JNK activity observed after P2Y$_6$R deletion in adipocytes improves whole body metabolism.

Strikingly, acute P2Y$_6$R activation in white adipocytes enhanced JNK phosphorylation, but this effect was absent in adipocytes lacking this receptor, indicating the specificity of JNK activation by P2Y$_6$R. Further, P2Y$_6$R activation resulted in increased phosphorylation of cJUN which acts downstream of JNK. Interestingly, chronic loss of P2Y$_6$R in WAT isolated from adipo-P2Y6$^{\Delta/\Delta}$ mice resulted in higher protein levels of T-JNK and T-cJUN and increased phosphorylation levels of these proteins. This observation is important, as chronic low-grade inflammation can regulate expression of total JNK in the hypothalamus (55).

In addition to JNK activation, we observed that P2Y$_6$R stimulation resulted in downstream binding of cJUN to the PPARα promoter, thereby reducing *PPARα* transcription in white adipocytes. Such regulation of *PPARα* transcription by cJUN has also been reported in cardiomyocytes (56). We also demonstrated that JNK activation downstream of the P2Y$_6$R regulates PPARα transcription, as treatment of cells with JNK inhibitor did not change *Ppara* mRNA levels. However, treatment of cells with JNK inhibitor in the presence of P2Y$_6$R agonist rescued the mRNA levels of *Ppara* decreased by receptor activation. P2Y$_6$R activation also decreased PPARα activity in white adipocytes, causing decreased expression of PGC1α, a coactivator of PPARα and master regulator of mitochondrial biogenesis (*SI Appendix,* Fig. S7).

We previously reported that P2Y$_6$R activation enhanced insulin-independent glucose uptake in C2C12 skeletal muscle cells via AMPK signaling (15). In this study, we deciphered the in vivo effect of P2Y$_6$R deficiency on skeletal muscle glucose metabolism. As expected, mice lacking skeletal muscle P2Y$_6$R showed impaired glucose tolerance and insulin sensitivity. In vitro studies confirmed that P2Y$_6$R stimulation increased glucose uptake independent of insulin signaling (*SI Appendix,* Fig. S7). These observations are in alignment with a recent study that reported improved glucose metabolism and enhanced glucose

uptake in skeletal muscle after activation of a G$_q$-coupled designer GPCR (57). Furthermore, impaired insulin tolerance in SM-P2Y6$^{\Delta/\Delta}$ mice was confirmed by decreased insulin-mediated glucose uptake in the gastrocnemius muscle lacking P2Y$_6$R.

To understand the interplay and contribution of adipose tissue and skeletal muscle P2Y$_6$R on systemic glucose homeostasis in obesity, we studied glucose metabolism in mice with global deletion of P2Y$_6$R maintained on an obesogenic diet. Improvement in glucose tolerance and insulin sensitivity were observed with no change in total body weight in WB-P2Y6$^{\Delta/\Delta}$ mice. These findings are consistent with the outcome of a recent study that reported improved insulin sensitivity in HFD mice lacking P2Y$_6$R in whole body or specifically in hypothalamic AgRP neurons (20). The role of P2Y$_6$R in controlling energy balance was also highlighted in a study demonstrating that increased plasma uridine levels in obesity increased hypothalamic UDP synthesis to activate AgRP P2Y$_6$R, thereby increasing food intake (11). Taken together, these observations indicate that P2Y$_6$R activation results in overall negative energy balance and impairment in glucose homeostasis. Importantly, our study provides convincing evidence that global lack of P2Y$_6$R improves the metabolic deficits associated with obesity and that adipose tissue is the major contributor to the improved systemic glucose metabolism.

Some limitations of this study should be noted. Due to the short half-life of MRS2578 (P2Y$_6$R antagonist) in aqueous medium we could not study the systemic effect over time of selective P2Y$_6$R blockade. Furthermore, although we have shown that MRS4383 is a selective agonist of P2Y$_6$R, it is not optimally designed for in vivo use, as it is a diphosphate derivative that is subject to hydrolysis by ectonucleotidases. Ongoing efforts in our laboratory are addressing this issue through the synthesis of novel P2Y$_6$R ligands. Clearly, this study provides a rational basis for the development of P2Y$_6$R antagonists for the treatment of obesity and T2D.

Materials and Methods

Mouse Models. Whole-body P2Y$_6$R KO mice (WB-P2Y6$^{\Delta/\Delta}$ mice) and mice with a loxP-flanked P2Y$_6$R allele (*P2Y6f/f*) have been described (17). Mice heterozygous for the P2Y$_6$R allele (WB-P2Y6$^{\Delta/WT}$) were intermated to generate experimental P2Y$_6$R KO mice (WB-P2Y6$^{\Delta/\Delta}$) and their wild-type (WT) littermates (WB-P2Y6$^{WT/WT}$, used as control). Mice were maintained on C57BL/6 background.

To generate mice lacking P2Y$_6$R selectively in adipocytes, we crossed P2Y$_6$R-floxed mice (M.I.'s laboratory, Freiburg, Germany) with *adipoq-Cre* mice expressing recombinase under the control of adiponectin promoter. *Adipoq-Cre* mice were purchased from The Jackson Laboratory (stock No. 010803; genetic background: C57BL/6J). Mice used for experiments were *P2Y6f/f* (control) and *adipoq-Cre$^{+/-}$P2Y6f/f* (adipo-P2Y6$^{\Delta/\Delta}$) mice. To generate mice lacking P2Y$_6$R selectively in skeletal muscle, we crossed P2Y$_6$R-floxed mice with mice expressing recombinase under the control of human skeletal actin promoter (*HSA-Cre 79*; The Jackson Laboratory [stock No. 006149]; genetic background: C57BL/6J). Mice used for experiments were *P2Y6f/f* (control) and *HSA-Cre$^{+/-}$P2Y6f/f* (SM-P2Y6$^{\Delta/\Delta}$) mice. All mouse experiments were approved by the National Institute of Diabetes and Digestive and Kidney Diseases (NIDDK) Intramural Research Program Animal Care and Use Committee, Protocol K083-LBC-17.

Mouse Maintenance and Diet-Induced Obesity. Adult male mice were used for all experiments reported in this study. Mice were kept on a 12-h light and 12-h dark cycle. Animals were maintained at room temperature (23 °C) on standard chow (7022 NIH-07 diet, 15% kcal fat, energy density 3.1 kcal/g, Envigo, Inc.). Mice had free access to food and water. To induce obesity, groups of mice were switched to a HFD (F3282, 60% kcal fat, energy density 5.5 kcal/gm, Bio-Serv) at 8 wk of age. Mice consumed the HFD for at least 8 wk, unless stated otherwise.

In Vivo Metabolic Phenotyping. Glucose tolerance tests (GTTs) were carried out in the morning on mice after a 12-h fast overnight. After checking fasted blood glucose levels, animals were intraperitoneally (i.p.) injected with glucose (1 or 2 g/kg as indicated) and blood was collected from tail vein at 15, 30, 60, and 120 min after injection. Blood glucose concentrations were determined using a

contour portable glucometer (Bayer). Insulin tolerance test (ITT) and pyruvate tolerance test (PTT) were carried out on mice fasted overnight for 12 h. Fasted blood glucose levels were determined, and then mice were injected i.p. with human insulin (0.75 or 1 U/kg; Humulin, Eli Lilly) or sodium pyruvate (2 g/kg), respectively, as indicated. Blood glucose levels were determined as described for GTT. All metabolic tests were performed with adult male mice that were more than 8 wk of age.

Body Composition Analysis. Mouse body mass composition (lean versus fat mass) was measured using a 3-in-1 Echo MRI Analyzer (Echo Medical System).

RNA Extraction and Gene Expression Analysis. Tissues from the killed mice were dissected and frozen rapidly on dry ice. Total RNA from tissues under analysis was extracted using the RNeasy mini kit (Qiagen). Total RNA (500 ng of RNA) was converted into cDNA using SuperScript III First-Strand Synthesis Super Mix (Invitrogen). Quantitative PCR was performed using the SYBR green method (Applied Biosystems). Gene expression was normalized to relative expression of 18s rRNA using the $\Delta\Delta$Ct method. A list of primer sequences used in this study is provided in *SI Appendix*, Table S3.

Plasma Metabolic Profiling. Blood was collected from the tail vein of mice in chilled K_2-ethylenediaminetetraacetic acid (EDTA)-containing tubes (RAM Scientific). Blood was collected from a group of mice that had free access to food (fed state) or from overnight fasted mice. Collected blood was centrifuged at 4 °C for 10 min at ~12,000 × g to obtain plasma. ELISA kit (Crystal Chem Inc.) was used to measure plasma insulin levels, following the manufacturer's instructions. Leptin and adiponectin levels were measured using ELISA kit from R&D Systems. Plasma glycerol, triglyceride, and FFA levels were determined using commercially available kits (Sigma-Aldrich).

Plasma Adipokine/Cytokine/Myokine Levels. Blood was collected from mice fed HFD for 8 to 10 wk. Blood was obtained from mandibular vein in chilled K_2-EDTA-containing tubes (RAM Scientific). Plasma was obtained by centrifugation of blood at 4 °C for 10 min at ~12,000 × g. Plasma adipokine and cytokine levels were measured using the Bio-Plex Multiplex Immunoassay System (Bio-Rad), following the manufacturer's instructions. Plasma myokines were measured using a Mouse Myokine Magnetic Bead panel (Millipore Sigma). The Luminex Milliplex Analyzer (Luminex) was used to determine the plasma concentrations, as described by the manufacturer.

Isolation, Culture, and Differentiation of White Adipocytes. To isolate mesenchymal stem cells from white fat depot, inguinal white fat pads of 6- to 8-wk-old male mice were dissected. Excised fat depot was minced into small pieces and digested at 37 °C for 45 min in Krebs-Ringer-Hepes-bicarbonate buffer (KRH buffer, 1.2 M NaCl, 40 mM KH_2PO_4, 20 mM $MgSO_4$, 10 mM $CaCl_2$, 100 mM $NaHCO_3$, 300 mM Hepes) containing 3.3 mg/mL collagenase I (Sigma-Aldrich). After digestion, 10 mL of KRH buffer was added and cell suspension was filtered through a 70-μm cell strainer, followed by centrifugation at 700 × g for 5 min at room temperature. Supernatant was discarded and the cell pellet was resuspended in KRH buffer and recentrifuged to obtain cell pellet of mesenchymal stem cells. The pellet was resuspended in Dulbecco's modified Eagle medium (DMEM) containing 10% fetal bovine serum (FBS) and 1% penicillin-streptomycin (Pen-Strep). Approximately 80,000 cells were seeded per well of collagen I-coated 12-well plates (Corning) and cultured at 37 °C, 10% CO_2. Cells were allowed to reach 100% confluency by replenishing media every second day. Two days after reaching confluence, cells were induced for differentiation using DMEM supplemented with 10% FBS, 1% Pen-Strep, 0.5 μM insulin, 250 μM 3-isobutyl-1-methylxanthine (IBMX), 2 μM troglitazone, 0.5 μM dexamethasone, and 60 μM indomethacin. After 72 h in induction media, cells were incubated in differentiation DMEM media supplemented with 10% FBS, 1% Pen-Strep, and 0.5 μM insulin for the next 72 h. Mature differentiated white adipocytes were used for further studies.

Isolation, Culture, and Differentiation of Brown Adipocytes. Brown preadipocytes were isolated from interscapular BAT of 3- to 4-wk-old mice. Excised BAT was cut in small pieces and digested at 37 °C for 30 min in KRH buffer, 1.2 M NaCl, 40 mM KH_2PO_4, 20 mM $MgSO_4$, 10 mM $CaCl_2$, 100 mM $NaHCO_3$, 300 mM Hepes) containing 3.3 mg/mL collagenase I (Sigma-Aldrich). After digestion, 10 mL of KRH buffer was added and filtered through a 70-μm cell strainer, followed by centrifugation at 900 × g for 5 min at room temperature. Cell pellet was washed once in 5 mL of KRH buffer, and cell pellet was resuspended in DMEM containing 10% FBS and 1% Pen-Strep. Cells were seeded in the collagen-I coated 12-well plates (Corning) and cultured at 37 °C,

10% CO_2. Media were changed every second day until cells reached 100% confluency. Differentiation was induced by added DMEM media supplemented with 2 μg/mL dexamethasone, 0.5 mM IBMX, 0.125 mM indomethacin, 20 nM insulin, and 1 nM T3 to the cells for 48 h. Cells were incubated with DMEM containing 10% FBS, 20 nM insulin, and 1 nM T3 for another 48 h. Mature brown adipocytes were used for experiments.

Isolation of Mature Adipocytes. The isolation of mature mouse adipocytes was performed as described previously (58). In brief, mouse fat pads were collected and digested with KRH buffer containing collagenase I (3 mg/mL). Digested tissues were filtered through a 250-μm cell strainer. After a 5-min centrifugation step at 700 rpm, the top layer containing mature adipocytes was collected and used for further experiments.

Western Blot Studies. Adipocyte cells/adipose tissues were homogenized in adipocyte lysis buffer (50 mM Tris, pH 7.4, 500 mM NaCl, 1% Nonidet P-40, 20% glycerol, 5 mM EDTA, and 1 mM phenylmethylsulfonyl fluoride [PMSF]) supplemented with EDTA-free protease inhibitor mixture and phosphatase inhibitors mixture (Roche). Tissue lysates were centrifuged at 14,000 rpm for 20 min at 4 °C twice before using the supernatant for Western blot studies. Protein concentrations in the lysates were determined using a bicinchoninic acid (BCA) assay kit (Pierce). Protein was denatured in NuPAGE LDS sample buffer (Thermo Fisher Scientific) and β-mercaptoethanol at 90 °C for 5 min (58, 59). Protein lysates were separated using 4 to 12% sodium dodecyl sulfate–polyacrylamide gel electrophoresis (Invitrogen) and transferred to nitrocellulose membranes (Bio-Rad). Membranes were incubated with primary antibody overnight at 4 °C in 5% wt/vol bovine serum albumin (BSA) prepared in 1× Tris-buffered saline with 0.1% Tween 20. The next day, the membranes were washed and incubated with hP-conjugated anti-rabbit/mouse secondary antibody. SuperSignal West Pico Chemiluminescent Substrate (Pierce) was used to visualize the bands on Azure Imager C600 (Azure Biosystems). Images were analyzed using ImageJ (NIH).

In Vivo [^{14}C]2-Deoxy-Glucose Uptake. To measure glucose uptake in vivo, mice on HFD for 20 wk were fasted overnight. Mice were injected with insulin (Humulin, 0.75 U/kg, i.p.) and a trace amount of [1-^{14}C]2-deoxy-D-glucose (10 μCi; PerkinElmer). After 40 min, mice were killed, and tissues were collected. Tissue weights were recorded, and tissues were homogenized. Radioactivity was measured and counted as described (60).

IP-One Quantification. Receptor-mediated intracellular changes in IP1 second messenger were measured using IP-One Gq kit (Cisbio) as per the manufacturer's instructions. Briefly, white or brown adipocytes were differentiated in 12-well plates as described before. Cells were serum starved for 4 h and treated with MRS4383 (1 μM) in stimulation buffer (pH 7.4) containing 50 mM LiCl. After 45 min of stimulation, cells were lysed using 200 μL of lysis buffer (Hepes buffer 1×, 1.5% Triton, O.2% BSA). Fourteen microliters of cell lysate was added to the 384-well low volume white microplates (Greiner Bio-One). Working solutions of IP1-d2 followed by Anti-IP1-Cryptate (3 μL) were added to the samples. Plate was sealed and incubated for 1 h at room temperature. Fluorescence was measured at 620 nm and 665 nm with the Mithras LB 940 multimode reader.

Histology of Fat Tissues and Liver. Different fat depots and liver were dissected out of mice and quickly frozen in liquid nitrogen/4% paraformaldehyde. The samples were sectioned and stained using standard techniques. H&E- and ORO-stained sections were visualized using a Keyence Microscope BZ-9000. Adipocyte images were analyzed for adipocyte size and number using Adiposoft software. Fixed adipose tissues were stained for F4/80 and UCP1 using standard immunohistochemistry methods. The stained images were visualized and captured using a Keyence Microscope BZ-9000.

C2C12 Growth and Differentiation. C2C12 is a mouse skeletal muscle cell line and is grown and differentiated according to American Type Culture Collection protocol. Briefly, C2C12 myoblast were cultured at 37 °C, 5% CO_2 in T75 flasks in DMEM supplemented with 5% FBS, 1% Pen-Strep. Cells were split after reaching 80% confluency into 12/24-well plates. Media were changed on alternate days until cells reached 80% confluency. Differentiation was started by replacing maintenance media with differentiation media (DMEM supplemented with 2% horse serum, 1% Pen-Strep). Myoblasts were differentiated for 7 d to convert them fully into elongated and contractile myotubes for experiments.

In Vitro Glucose Uptake in C2C12 Cells. C2C12 myoblasts were differentiated into myotubes in 12-well plates. The 2-deoxy-glucose uptake in myotubes was measured with modifications as described previously (15). Briefly, C2C12 myotubes were serum deprived in DMEM low glucose media for 3 h. Myotubes were treated with P2Y$_6$R antagonist (MRS2578, 1,4-di-[(3-iso-thiocyanatophenyl)-thioureido]butane, 1 μM) in wells as indicated for 30 min. Insulin (100 nM) and P2Y$_6$R agonist MRS4383 (1 μM) were added to indicated wells for an additional 30 min. After drug treatment, 0.35 mL of transport solution with 0.5 μCi/mL [^{3}H]2-deoxy-glucose (PerkinElmer) was added to the cells for 5 min. Cells were washed with ice-cold stop solution (0.9% saline) and aspirated to dryness. One milliliter of 0.05 N NaOH was added to each well of a 12-well plate and radioactivity was measured using a scintillation counter. Results were calculated as 2-DG/mg protein/min uptake. Specific uptake in the absence of any stimulation was defined as basal uptake. Data are expressed as percent of basal uptake. To overexpress P2Y$_6$R in myotubes, an adenovirus (Ad-GFP-m-P2RY6, Vector Biolabs) was added to myotubes 24 h after inducing differentiation at the multiplicity of infection (MOI) of 250. Cells were differentiated for another 5 d before performing glucose uptake studies.

High Throughput RNA Sequencing. Adipose tissues were dissected out from mice maintained on HFD for 8 wk and snap frozen in liquid nitrogen. Total RNA from fat tissues was extracted using the RNeasy mini kit (Qiagen). Quantity and quality of RNA were checked using the Agilent Bioanalyzer system. RNA with RNA integrity number >8 was used to prepare transcriptomic libraries using the NEBNext Ultra RNA library prep kit (New England Biolabs). High throughput RNA sequencing (RNA-seq) was performed at the NIDDK Genomic Core Facility (NIH) using the HiSeq 2500 instrument (Illumina). Raw sequences were passed through quality control and mapped to mouse (mm9) genome. Differential gene expression analysis was performed using the Genomatix Genome analyzer with log2 (fold change) cutoff of ±0.58. Biological pathway and enrichment analysis were performed using Metacore (version 6.32, Thomson Reuters) and Ingenuity pathway analysis (Qiagen). The RNA-seq data have been deposited in National Center for Biotechnology Information (NCBI) Sequence Read Archive (PRJNA607327 and PRJNA607321).

CHIP Assay. Differentiated mouse white adipocytes were treated with P2Y$_6$R agonist as indicated. After stimulation for 2 h, cells were fixed with form-aldehyde, and ChIP assays were performed using the Abcam ChIP kit (ab500) following the manufacturer's instructions. Antibodies against cJUN was used to immunoprecipitate cJUN-bound promoter regions. Subsequently, PCR was performed on the eluted DNA using primers annealing to the mouse *PPARa* gene promoter region. Primer sequences used for PCR analysis are listed in *SI Appendix*, Table S3.

Luciferase Assay. Astrocytoma 1321N1 cells stably expressing the human P2Y$_6$R were transiently transfected with DR-1, β-galactosidase with or without PPARα, RXRα-expressing DNA plasmids using Lipofectamine 2000. Cells were treated 48 h after transfection with MRS4383 as indicated. Cells were harvested 6 h after stimulation and luciferase activity was measured according to the manufacturer's protocol (Promega). Relative luciferase activity was normalized to the β-galactosidase activity measured using multi-mode plate reader (SpectraMax M5, Molecular Devices) for each sample using the manufacturer's protocol (Promega).

Indirect Calorimetry. Energy expenditure (O$_2$ consumption/CO$_2$ production), food intake, and respiratory exchange ratio were measured in mice housed at 22 °C using an Oxymax-CLAMS (Columbus Instruments) monitoring system. Before moving mice to HFD feeding, mice were maintained on CD for 3 d. On day 4, mice were transferred to HFD and data were collected after every 4 min (total 11 chambers). Mice were maintained on HFD for 4 additional days before ending the experiment. Water and food were provided ad libitum.

Statistics. Data are expressed as mean + SEM for the number of observations indicated. Data were tested by two-way ANOVA, followed by post hoc tests or by two-tailed unpaired Student's *t* test, as appropriate. Energy expenditure data were analyzed using analysis of covariance (ANCOVA). A *P* value of <0.05 was considered statistically significant.

Study Approval. All animal studies were carried out according to the NIH Guidelines for Animal Research and approved by the NIDDK Institutional Animal Care and Use Committee.

Data Availability. All data needed to evaluate the conclusions in the paper are present in the paper and/or *SI Appendix*. Additional data related to this paper may be requested from the authors. RNA-seq data have been deposited in NCBI Sequence Read Archive (PRJNA607327 and PRJNA607321).

1. D. Segula, Complications of obesity in adults: A short review of the literature. *Malawi Med. J.* **26**, 20–24 (2014).
2. T. W. Stone, L. McPherson, L. Gail Darlington, Obesity and cancer: Existing and new hypotheses for a causal connection. *EBioMedicine* **30**, 14–28 (2018).
3. J. O. Hill, H. R. Wyatt, J. C. Peters, Energy balance and obesity. *Circulation* **126**, 126–132 (2012).
4. E. D. Rosen, B. M. Spiegelman, What we talk about when we talk about fat. *Cell* **156**, 20–44 (2014).
5. S. E. Shoelson, L. Herrero, A. Naaz, Obesity, inflammation, and insulin resistance. *Gastroenterology* **132**, 2169–2180 (2007).
6. N. Ouchi, J. L. Parker, J. J. Lugus, K. Walsh, Adipokines in inflammation and metabolic disease. *Nat. Rev. Immunol.* **11**, 85–97 (2011).
7. H. Wu, C. M. Ballantyne, Skeletal muscle inflammation and insulin resistance in obesity. *J. Clin. Invest.* **127**, 43–54 (2017).
8. M. P. Abbracchio *et al*., International union of pharmacology LVIII: Update on the P2Y G protein-coupled nucleotide receptors: From molecular mechanisms and patho-physiology to therapy. *Pharmacol. Rev.* **58**, 281–341 (2006).
9. E. R. Lazarowski, R. C. Boucher, T. K. Harden, Mechanisms of release of nucleotides and integration of their action as P2X- and P2Y-receptor activating molecules. *Mol. Pharmacol.* **64**, 785–795 (2003).
10. D. Communi, R. Janssens, N. Suarez-Huerta, B. Robaye, J. M. Boeynaems, Advances in signalling by extracellular nucleotides. the role and transduction mechanisms of P2Y receptors. *Cell. Signal.* **12**, 351–360 (2000).
11. S. M. Steculorum *et al*., Hypothalamic UDP increases in obesity and promotes feeding via P2Y6-dependent activation of AgRP neurons. *Cell* **162**, 1404–1417 (2015).
12. P. Badillo *et al*., High plasma adenosine levels in overweight/obese pregnant women. *Purinergic Signal.* **13**, 479–488 (2017).
13. M. A. Laplante, L. Monassier, M. Freund, P. Bousquet, C. Gachet, The purinergic P2Y1 receptor supports leptin secretion in adipose tissue. *Endocrinology* **151**, 2060–2070 (2010).
14. J. Xu *et al*., GPR105 ablation prevents inflammation and improves insulin sensitivity in mice with diet-induced obesity. *J. Immunol.* **189**, 1992–1999 (2012).
15. R. Balasubramanian, B. Robaye, J. M. Boeynaems, K. A. Jacobson, Enhancement of glucose uptake in mouse skeletal muscle cells and adipocytes by P2Y6 receptor agonists. *PLoS One* **9**, e116203 (2014).
16. Z. Zhang *et al*., P2Y(6) agonist uridine 5'-diphosphate promotes host defense against bacterial infection via monocyte chemoattractant protein-1-mediated monocytes/macrophages recruitment. *J. Immunol.* **186**, 5376–5387 (2011).
17. I. Bar *et al*., Knockout mice reveal a role for P2Y6 receptor in macrophages, endothelial cells, and vascular smooth muscle cells. *Mol. Pharmacol.* **74**, 777–784 (2008).
18. A. K. Riegel *et al*., Selective induction of endothelial P2Y6 nucleotide receptor promotes vascular inflammation. *Blood* **117**, 2548–2555 (2011).
19. M. Nishida *et al*., P2Y6 receptor-Galpha12/13 signalling in cardiomyocytes triggers pressure overload-induced cardiac fibrosis. *EMBO J.* **27**, 3104–3115 (2008).
20. S. M. Steculorum *et al*., Inhibition of P2Y6 signaling in AgRP neurons reduces food intake and improves systemic insulin sensitivity in obesity. *Cell Rep.* **18**, 1587–1597 (2017).
21. D. Wanders, E. C. Graff, R. L. Judd, Effects of high fat diet on GPR109A and GPR81 gene expression. *Biochem. Biophys. Res. Commun.* **425**, 278–283 (2012).
22. S. J. Paulsen *et al*., Expression of the fatty acid receptor GPR120 in the gut of diet-induced-obese rats and its role in GLP-1 secretion. *PLoS One* **9**, e88227 (2014).
23. D. Osei-Hyiaman *et al*., Endocannabinoid activation at hepatic CB1 receptors stimulates fatty acid synthesis and contributes to diet-induced obesity. *J. Clin. Invest.* **115**, 1298–1305 (2005).
24. L. Chen, R. Chen, H. Wang, F. Liang, Mechanisms linking inflammation to insulin resistance. *Int. J. Endocrinol.* **2015**, 508409 (2015).
25. K. S. Toti *et al*., Pyrimidine nucleotides containing a (S)-methanocarba ring as P2Y6 receptor agonists. *MedChemComm* **8**, 1897–1908 (2017).
26. J. H. Stern, J. M. Rutkowski, P. E. Scherer, Adiponectin, leptin, and fatty acids in the maintenance of metabolic homeostasis through adipose tissue crosstalk. *Cell Metab.* **23**, 770–784 (2016).
27. T. Müller *et al*., P2Y6 receptor activation promotes inflammation and tissue remodeling in pulmonary fibrosis. *Front. Immunol.* **8**, 1028 (2017).

PHYSIOLOGY

28. L. Bellocchio et al., Sustained Gq-protein signaling disrupts striatal circuits via JNK. J. Neurosci. **36**, 10611–10624 (2016).

29. J. Hirosumi et al., A central role for JNK in obesity and insulin resistance. Nature **420**, 333–336 (2002).

30. C. J. Pol et al., Cardiac myocyte KLF5 regulates body weight via alteration of cardiac FGF21. Biochim. Biophys. Acta Mol. Basis Dis. **1865**, 2125–2137 (2019).

31. D. J. Mangelsdorf et al., The nuclear receptor superfamily: The second decade. Cell **83**, 835–839 (1995).

32. J. He, S. Watkins, D. E. Kelley, Skeletal muscle lipid content and oxidative enzyme activity in relation to muscle fiber type in type 2 diabetes and obesity. Diabetes **50**, 817–823 (2001).

33. B. Nyholm et al., Evidence of an increased number of type IIb muscle fibers in insulin-resistant first-degree relatives of patients with NIDDM. Diabetes **46**, 1822–1828 (1997).

34. F. Reimann, F. M. Gribble, G protein-coupled receptors as new therapeutic targets for type 2 diabetes. Diabetologia **59**, 229–233 (2016).

35. T. Gnad et al., Adenosine/A2B receptor signaling ameliorates the effects of aging and counteracts obesity. Cell Metab. **32**, 56–70 e7 (2020).

36. T. Gnad et al., Adenosine activates brown adipose tissue and recruits beige adipocytes via A2A receptors. Nature **516**, 395–399 (2014).

37. S. Koizumi et al., UDP acting at P2Y6 receptors is a mediator of microglial phagocytosis. Nature **446**, 1091–1095 (2007).

38. D. M. Grbic, E. Degagné, C. Langlois, A. A. Dupuis, F. P. Gendron, Intestinal inflammation increases the expression of the P2Y6 receptor on epithelial cells and the release of CXC chemokine ligand 8 by UDP. J. Immunol. **180**, 2659–2668 (2008).

39. G. R. Somers, F. M. Hammet, L. Trute, M. C. Southey, D. J. Venter, Expression of the P2Y6 purinergic receptor in human T cells infiltrating inflammatory bowel disease. Lab. Invest. **78**, 1375–1383 (1998).

40. K. Klepac et al., The Gq signalling pathway inhibits brown and beige adipose tissue. Nat. Commun. **7**, 10895 (2016).

41. D. C. da Costa, A. M. Landeira-Fernandez, Thermogenic activity of the Ca2+-ATPase from blue marlin heater organ: Regulation by KCl and temperature. Am. J. Physiol. Regul. Integr. Comp. Physiol. **297**, R1460–R1468 (2009).

42. K. Ikeda et al., UCP1-independent signaling involving SERCA2b-mediated calcium cycling regulates beige fat thermogenesis and systemic glucose homeostasis. Nat. Med. **23**, 1454–1465 (2017).

43. A. Brunschweiger, C. E. Müller, P2 receptors activated by uracil nucleotides–An update. Curr. Med. Chem. **13**, 289–312 (2006).

44. H. Eshima, D. C. Poole, Y. Kano, In vivo calcium regulation in diabetic skeletal muscle. Cell Calcium **56**, 381–389 (2014).

45. A. K. Cardozo et al., Cytokines downregulate the sarcoendoplasmic reticulum pump Ca2+ ATPase 2b and deplete endoplasmic reticulum Ca2+, leading to induction of endoplasmic reticulum stress in pancreatic beta-cells. Diabetes **54**, 452–461 (2005).

46. M. Luo, M. E. Anderson, Mechanisms of altered Ca2+ handling in heart failure. Circ. Res. **113**, 690–708 (2013).

47. H. Shi, Y. D. Halvorsen, P. N. Ellis, W. O. Wilkison, M. B. Zemel, Role of intracellular calcium in human adipocyte differentiation. Physiol. Genomics **3**, 75–82 (2000).

48. M. B. Zemel, H. Shi, B. Greer, D. Dirienzo, P. C. Zemel, Regulation of adiposity by dietary calcium. FASEB J. **14**, 1132–1138 (2000).

49. I. C. Ho, J. H. Kim, J. W. Rooney, B. M. Spiegelman, L. H. Glimcher, A potential role for the nuclear factor of activated T cells family of transcriptional regulatory proteins in adipogenesis. Proc. Natl. Acad. Sci. U.S.A. **95**, 15537–15541 (1998).

50. R. L. Byyny, M. LoVerde, S. Lloyd, W. Mitchell, B. Draznin, Cytosolic calcium and insulin resistance in elderly patients with essential hypertension. Am. J. Hypertens. **5**, 459–464 (1992).

51. L. Ozcan et al., Calcium signaling through CaMKII regulates hepatic glucose production in fasting and obesity. Cell Metab. **15**, 739–751 (2012).

52. G. Sabio et al., A stress signaling pathway in adipose tissue regulates hepatic insulin resistance. Science **322**, 1539–1543 (2008).

53. G. Tuncman et al., Functional in vivo interactions between JNK1 and JNK2 isoforms in obesity and insulin resistance. Proc. Natl. Acad. Sci. U.S.A. **103**, 10741–10746 (2006).

54. X. Zhang et al., Selective inactivation of c-Jun NH2-terminal kinase in adipose tissue protects against diet-induced obesity and improves insulin sensitivity in both liver and skeletal muscle in mice. Diabetes **60**, 486–495 (2011).

55. R. Rorato et al., LPS-induced low-grade inflammation increases hypothalamic JNK expression and causes central insulin resistance irrespective of body weight changes. Int. J. Mol. Sci. **18**, E1431 (2017).

56. K. Drosatos et al., Cardiac myocyte KLF5 regulates Ppara expression and cardiac function. Circ. Res. **118**, 241–253 (2016).

57. D. B. J. Bone et al., Skeletal muscle-specific activation of G_q signaling maintains glucose homeostasis. Diabetes **68**, 1341–1352 (2019).

58. S. P. Pydi et al., Beta-arrestin-2 is essential for maintaining whole body glucose and energy homeostasis. Nat. Commun. **10**, 2936 (2019).

59. S. P. Pydi et al., Adipocyte β-arrestin-1 suppresses myogenic reprogramming of brown fat to maintain euglycemia. Sci. Adv. **6**, eaba1733 (2020).

60. J. K. Kim, O. Gavrilova, Y. Chen, M. L. Reitman, G. I. Shulman, Mechanism of insulin resistance in A-ZIP/F-1 fatless mice. J. Biol. Chem. **275**, 8456–8460 (2000).